RSC Advances

PAPER

View Article Online
View Journal | View Issue

Cite this: *RSC Adv.*, 2026, **16**, 14535

Catalytic performance and SERS substrate efficiency of PdNPs@GOQDs

T. P. Amrutha,[a] T. P. Arathi,[a] Ritu Gopal,[a] P. B. Arya,[a] V. Nidhisha,[a] C. Anjali,[a] T. D. Suja,[a] K. R. Sunaja Devi,[b] Suja Haridas[c] and Renuka Neeroli Kizhakayil *[a]

Received 25th October 2025
Accepted 8th March 2026

DOI: 10.1039/d5ra08190d

rsc.li/rsc-advances

Graphene Oxide Quantum Dots (GOQDs) have received significant attention for diverse applications owing to their unique physical and chemical properties. Herein, yellow luminescent graphene oxide quantum dots are achieved *via* hydrothermal pathway and are characterized using different analytical methods. GOQDs, noted for their reducing character, are utilized for the synthesis of palladium nanoparticles (PdNPs). PdNPs@GOQDs obtained are explored for their catalytic efficiency and SERS substrate performance. The combined effect of electromagnetic enhancement and chemical enhancement factors make the composite a good SERS substrate, as exemplied using Rhodamine B molecule. PdNPs@GOQDs exhibited catalytic activity that effectively promoted the reduction of several functionalized aromatic nitroarenes. Notably, sensitive groups like nitrile and ester were well-tolerant under the reaction conditions, warranting the potential of the system in synthesising amines of industrial and environmental significance with high selectivity.

1 Introduction

Graphene quantum dots (GQDs), and its oxidized analogues, Graphene Oxide Quantum Dots (GOQDs) have captured significant attention of the researchers for their multifaceted applications. The quantum confinement, along with variations in size, shape and edge structure, significantly impact their electrical and optical properties. Consequently, GQDs and GOQDs hold great potential for optical and electrochemical sensing, photovoltaics, photocatalysis, bioimaging, biosensing, LEDs and plasmonics.[1,2] Additionally, the presence of surface oxygen functionalities and electron exchange properties make them excellent catalysts and reducing agents.[3,4] In the present study, Graphene Oxide Quantum Dots are explored for their potential as Surface Enhanced Raman Spectroscopy (SERS) substrate and reductant.

SERS stands out as a promising analytical tool that enables the detection of analyte molecules with chemical specificity.[5–7] Typically, SERS-active substrates are created using "roughened" nanostructured patterned surfaces. Noble metals and transition metals are widely studied in this direction.[8–10] For further signal enhancement, often metals have been combined with semiconductors, piezoelectric polymers and carbon-based materials to create hybrid nanomaterials.[6,11–13] Graphene and its derivatives are much explored SERS platforms among the carbon species.[14–16] Compared to the conventional graphene sheets, GQDs/GOQDs with larger specific surface areas and more accessible edges facilitate more efficient adsorption of target molecules.[17,18] Liu *et al.*, have reported the SERS substrate activity of GQDs achieved using plasma chemical vapour deposition.[19] It was noted that the SERS signal is facilitated by the electron charge transfer between the hydrogen bonding sites on the edge of GQDs and hydroxyl molecules of the analyte. Heteroatom doping, particularly, 'N' atom incorporation, is identified as an attractive solution to tune the material properties of the GQDs. Das *et al.*, have synthesized nitrogen GQDs (N-GQDs), which exhibited high sensitivity for rhodamine detection, operating *via* a charge transfer process between N-GQDs and rhodamine molecules.[20] Laser induced ionization processing[21] and electrochemical methods[22] are also used for achieving GQDs that are active as SERS substrates. GQDs assembled nanotubes were achieved by Cheng *et al.* as SERS substrate using template assisted electrodeposition process.[17] Mary *et al.* have conducted a computational investigation on duphaston (DPH) detection using undoped and doped GQDs, and concluded that DPH works on the electrophilic site of nanoclusters as donor of electrons.[23] Theoretical investigation was also conducted in ultrasensitive detection of melamine on sulphur and oxygen doped GQDs.[15]

The second application of GOQDs probed here, vis., the reducing nature, is based on the electron exchange capability of these particles. GQDs and GOQDs, falling under the broad category of carbon dots, have also been recognized for their reducing properties, especially for the synthesis of metal nanoparticles from metal salt precursors. Metal nanoparticles

[a]*Department of Chemistry, University of Calicut, Kerala 673635, India. E-mail: renuka@uoc.ac.in*

[b]*Department of Chemistry, CHRIST (Deemed to be University), Bengaluru, Karnataka 560029, India*

[c]*Department of Applied Chemistry, Cochin University of Science and Technology, Kerala 682022, India*

are typically synthesized by reducing metal salt solutions, a process that involves reducing agents like sodium borohydride and citrate under harsh reaction conditions. Additionally, capping agents are commonly used to stabilize the nanoparticles.[24] Previous studies have shown that GQDs are effective electron donors and can serve as reducing agents for noble metal ions, resulting in the formation of GQDs@noble metal nanoparticle composite material, that has drawn immense attention from the researchers.[25] Here GOQDs are identified as an excellent reductant for achieving palladium nanoparticles (PdNPs) from Pd(II) precursor. GOQDs and carbon dots have been explored for the synthesis of PdNPs previously. Photochemical method has been utilized for the synthesis of Pd/carbon dots by Dhenadhayalan *et al.*[26] Selim *et al.* have prepared a polyamide cross linked carbon dot and used it for the subsequent deposition of PdNPs by treatment with $PdCl_2$ under refluxing in ethanol.[27] The obtained Pd NP-carbon dot systems have established themselves as excellent catalysts for various organic reactions. It is proven that carbon dot-palladium-nanoparticle composite exhibits high catalytic activity for the Heck and Suzuki coupling reactions.[28] Keshipour *et al.* synthesized Pd(0) supported on N-doped graphene quantum dot (N-GQD) modified cellulose from $PdCl_2$ using $NaBH_4$ as reducing agent and employed for catalytic reduction of nitroaromatics.[29] Thermolytic reduction of $PdCl_2$ in the presence of GQDs also yielded GQDs-supported palladium nanoparticles.[30]

In the present work, yellow luminescent nitrogen doped graphene oxide quantum dots (GOQDs) are synthesized from *ortho*-phenylenediamine *via* hydrothermal route, and are well characterized using various analytical tools. GOQDs performed as a SERS active material, as exemplified by the signal enhancement of Rhodamine B (RhB). The system also served as a reducing and capping agent in the synthesis of palladium nanoparticles (PdNPs) from Pd(II) precursor under ambient conditions. PdNPs@GOQDs are examined for their SERS substrate performance as well as catalytic efficiency towards nitroarene reduction.

2 Experimental

2.1 Materials

Analytical grade reagents were used for the study and was used as-received. *Ortho* phenylenediamine was purchased from Thermo Scientific. Palladium(II) acetate was received from BLD Pharmatech Pvt. Ltd. Sodium borohydride and silica were obtained from Spectrochem Pvt. Ltd. Rhodamine B, nitrobenzene, 4-nitrobenzonitrile, 3-nitroacetophenone, 1-nitronaphthalene and methyl 4-nitrobenzoate were supplied by HiMedia Laboratories Pvt. Ltd. Ethyl acetate and magnesium sulphate were purchased from Merck Ltd. Hexane and dichloromethane were obtained from Qualigens. Deionized (DI) water was used to make the solutions for the studies and used as a solvent for the reduction reaction.

2.2 Synthesis of GOQDs and PdNPs@GOQDs

200 mg of *ortho*-phenylenediamine was dissolved in 60 mL of water and was subjected to hydrothermal treatment at 200 °C for 6 hours in a Teflon-lined autoclave. After cooling to room temperature, the insoluble fraction was filtered out. The GOQDs were then separated by centrifugation at 3500 rpm for 30 minutes, followed by dialysis, and stored at 4 °C for subsequent studies (Scheme 1).

100 μL of GOQDs and 300 μL of 0.05 M palladium(II) acetate solutions were added to 5 mL DI water at laboratory conditions. The orange solution turned into brown within ~10 minutes, indicating the formation of palladium nanoparticles. The solid separated was then dried at 60 °C to obtain PdNPs@GOQDs.

2.3 SERS measurement

The SERS substrate was fabricated by dipping the glass plate in 10 mL of the as-prepared GOQDs/PdNPs@GOQDs and drying in an oven at 60 °C. 20 μL of RhB solution of different concentrations were dropped on the top of substrate coated glass plate and dried under room temperature for the SERS analysis. After the analyte detection, the substrate is exposed to photons using Xenon lamp. This leads to photodegradation of the dye, regenerating the SERS platform.

2.4 Nitrophenol reduction reaction

Nitrophenol reduction was conducted to examine the catalytic efficiency of PdNPs@GOQDs, which was monitored using UV visible spectroscopy. 100 μM solution (1.7 mL) of 4-nitrophenol (4-NP) solution was treated with 100 μL of $NaBH_4$ (10 mM) solution for affecting the conversion of nitro phenol into nitrophenolate ion, which affected the colour change of the

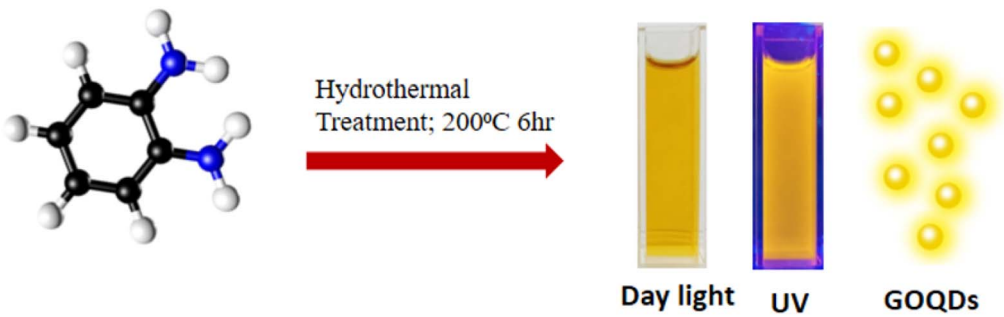

Scheme 1 Schematic illustration of synthesis of GOQDS by hydrothermal treatment.

solution to bright yellow, with characteristic absorbance at 400 nm. 100 μL of PdNPs@GOQDs were introduced to the said solution. Decrease in the absorbance at this wavelength concomitant with the formation of a new peak around 292 nm indicating the formation of 4-amino phenol (4-AP).

2.5 Hydrogenation of nitroarenes using PdNPs@GOQDs

The objective was to explore the catalytic ability of the PdNPs@GOQDs catalyst for the reduction of nitroarenes under eco-friendly conditions. Therefore, the feasibility of the reduction in aqueous medium was explored. The amount of $NaBH_4$ typically required was 2 molar equivalents and the same was used throughout the study. TLC analysis of the reaction mixture revealed that the reduction is fast and typically went to completion in 30 minutes. Nitroarene (0.25 mmol) and sodium borohydride (0.5 mmol) were suspended in de-ionized water (2 mL) in a 25 mL round bottom flask. 10 mg of PdNPs@GOQDs was added and the reaction mixture was stirred on a magnetic stirrer at room temperature. The optimized catalyst loading was 10 mg of PdNPs@GOQDs for 0.25 mmol of the nitroarene. At a lower catalyst loading (5 mg/0.25 mmol), the efficiency of the reduction was reduced to 75% of the value obtained when 10 mg loading was done.

When the reaction was complete (TLC analysis), the reaction mixture was partitioned between water and dichloromethane (10 mL). The organic layer was separated and the aqueous layer was extracted with dichloromethane. The combined organic layer was dried over anhydrous magnesium sulphate, filtered and evaporated to dryness on a rotavapor. The residue was as purified by column chromatography on alumina using hexane–ethyl acetate mixture as eluent to afford analytically pure samples of the aniline derivatives.

2.6 Characterisations

The morphology and particle size were analyzed by JEOL JEM 2100 transmission electron microscopy (TEM) running at an accelerating voltage of 200 kV. The average particle size was determined from TEM image by assessing particle size distribution determined using image J software. Fluorescence of the material under UV illumination was monitored using LZC-4X photoreactor. Raman spectra were recorded using WITec alpha 300RRA (WITec GmbH, Ulm, Germany) having 532 nm DPSS laser. Omicron spectrometer was used to perform X-ray photoelectron spectroscopy (XPS) analysis with Mg K_α radiation having an energy of 1253 eV. The UV-vis absorption spectrum was measured with a JASCO V-550 spectrometer. The fluorescence spectrometer Cary Eclipse (Agilent Technology) was used to record the fluorescence spectra of GOQDs solution. HORIBA time-correlated single-photon-counting (TCSPC) with 370 nm wavelength excitation light source was used to measure fluorescence lifetime decay. X-ray diffraction (XRD) pattern of the systems was recorded using a Rigaku Miniflex-II diffractometer with Cu K_α radiation in the scan range of 2θ 5–90°. JASCO FTIR-4100 spectrometer was used to obtain the Fourier transformn infrared (FTIR) spectrum using the KBr pellet technique. Proton Nuclear Magnetic Resonance (^{1}HNMR) spectra were measured using Jeol@400 Spectrometer.

3 Results and discussion

3.1 Characterisation of GOQDs

Hydrothermal treatment of *ortho* phenylenediamine resulted in yellow luminescent GOQDs (Scheme 1). The possible mechanism of formation of GOQDs are given in Fig. S1, SI.[31] XRD analysis confirms the crystalline structure of the sample (Fig. 1a). The most intense peak appears at 2θ value of 8.5°, indicating the (001) lattice plane with *d*-spacing of 1.03 nm. Another peak is observed at 17.5°, corresponding to *d*-spacing 0.51 nm, which represents the (002) plane. These peaks are in accordance with the peaks of GOQDs reported previously.[32,33] The sharp nature of peaks when compared to the previous ones shows the significant ordering of carbon planes. Additionally, a peak at 44.5° is seen in the XRD pattern of GOQDs, corresponding to *d*-spacing of 0.2 nm indicating the (100) lattice plane. The morphology and size of the GOQDs were examined using TEM (Fig. 1b–d). The HR-TEM image provided in Fig. 1b confirms the spherical shape of the sample, while the polycrystalline nature is demonstrated by the Selective Area Diffraction (SAED) pattern (Fig. 1c). The *d*-spacing value derived from the SAED pattern aligns well with the (100) interplanar distance obtained from the XRD analysis of the system. The inset of Fig. 1b shows lattice fringes with *d*-spacing value of 0.19 nm. Fig. 1d shows an average particle size of 2.2 nm, as indicated by the particle size distribution histogram. Figure (Fig. S2, SI) shows the AFM image of the system, which justified the lateral size and the height profile (<2 nm) indicated mono layer nature of GOQDs.

The FTIR spectrum of GOQDs (Fig. 1e) displays a broad band between 3100 and 3800 cm^{-1}, indicating the presence of oxygen functional groups within the carbon matrix, which accounts for the hydrophilicity of particles. The peak at 2339 cm^{-1} is attributed to the C≡N stretching vibrations.[34] The broad band centered at 2084 cm^{-1} represents the weak stretching vibration of C≡C groups.[35] The band at 1439 cm^{-1} is due to the symmetrical deformations of CH_3 and in-plane deformations of O–H. The band observed at 1383 cm^{-1} corresponds to the stretching modes of C=N/C–N bonds.[36] The band around 1636 cm^{-1} corresponds to C=C vibrations in the aromatic carbon framework. Other functional groups also contribute to the absorption in this range, including C=O vibrations of amide groups (imide bands), non-aromatic double bonds, hydrogen bonds involving C=O groups in ketones and quinones, and symmetrical stretching of the COO^- group. The spectral band at 620 cm^{-1} results from the angular deformations outside C–H aromatic rings, and the peak at 1032 cm^{-1} is assigned to C–O vibrations within C–O–C groups.[35,37] Substantial functionalization of GOQDs is further supported by these findings.

Fig. 1f displays the Raman spectrum of GOQDs, revealing information about the conjugated carbon–carbon double bonds that produce intense peaks. The G band, located at 1516 cm^{-1}, corresponds to the E_{2g} phonon of sp^2 carbon atoms, while the D

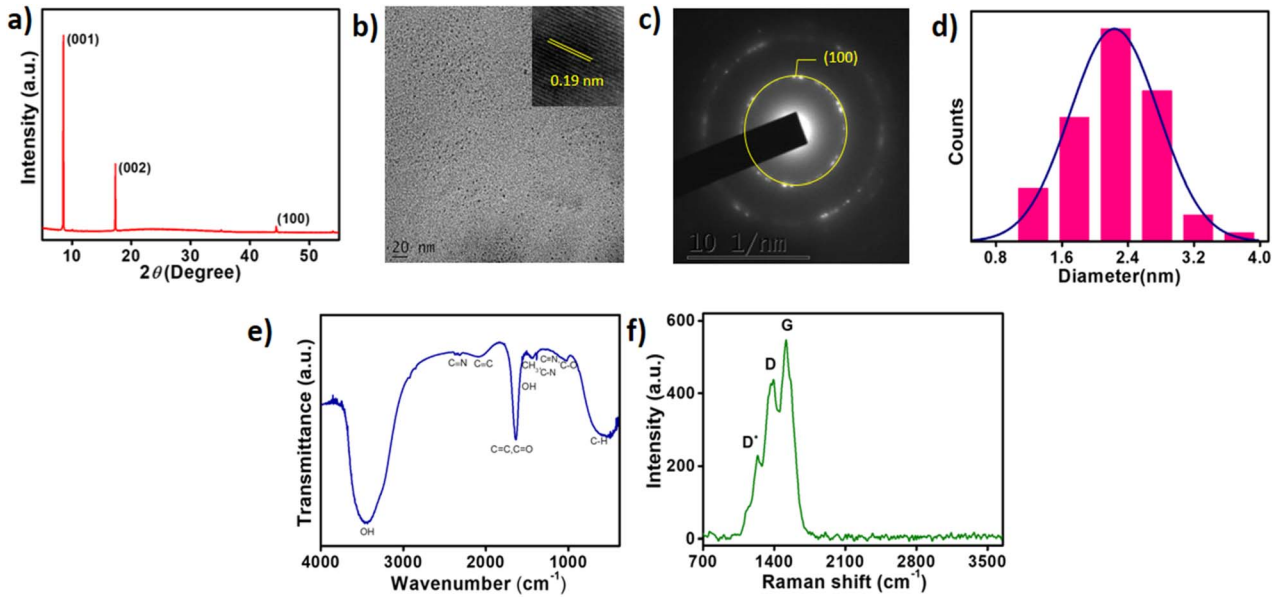

Fig. 1 (a) XRD pattern of GOQDs. (b) HR-TEM image; inset shows lattice fringes. (c) SAED pattern. (d) Size distribution histogram obtained from the TEM image. (e) FTIR spectrum of GOQDs. (f) Raman spectrum of GOQDs.

band positioned at 1391 cm^{-1}, indicates the breathing mode of *k*-point phonons with A_{1g} symmetry. These D and G bands represent vibrations in sp^3 and sp^2 carbon atoms, respectively. The G band is associated with the vibration of sp^2 carbon atoms in the two-dimensional hexagonal graphitic lattice, while the D band indicates disorder due to defects The intensity ratio of these bands, I_D/I_G, is crucial for assessing the factors such as vacancies, grain boundaries and amorphous carbon species disorder in carbon matrix. Here, the intensity ratio is 0.82, suggesting a predominance of sp^2 carbon domains over sp^3 carbon structures.[4,38] An additional band at 1239 cm^{-1}, labelled D*, arises from the vibrations of carbon atoms constrained by oxygen-containing groups.[39]

Fig. 2a shows the UV-vis absorption spectrum of the GOQDs. The peaks at 205 and 235 nm represent the π–π* transitions of aromatic C=C bonds, while the peak at 288 nm corresponds to

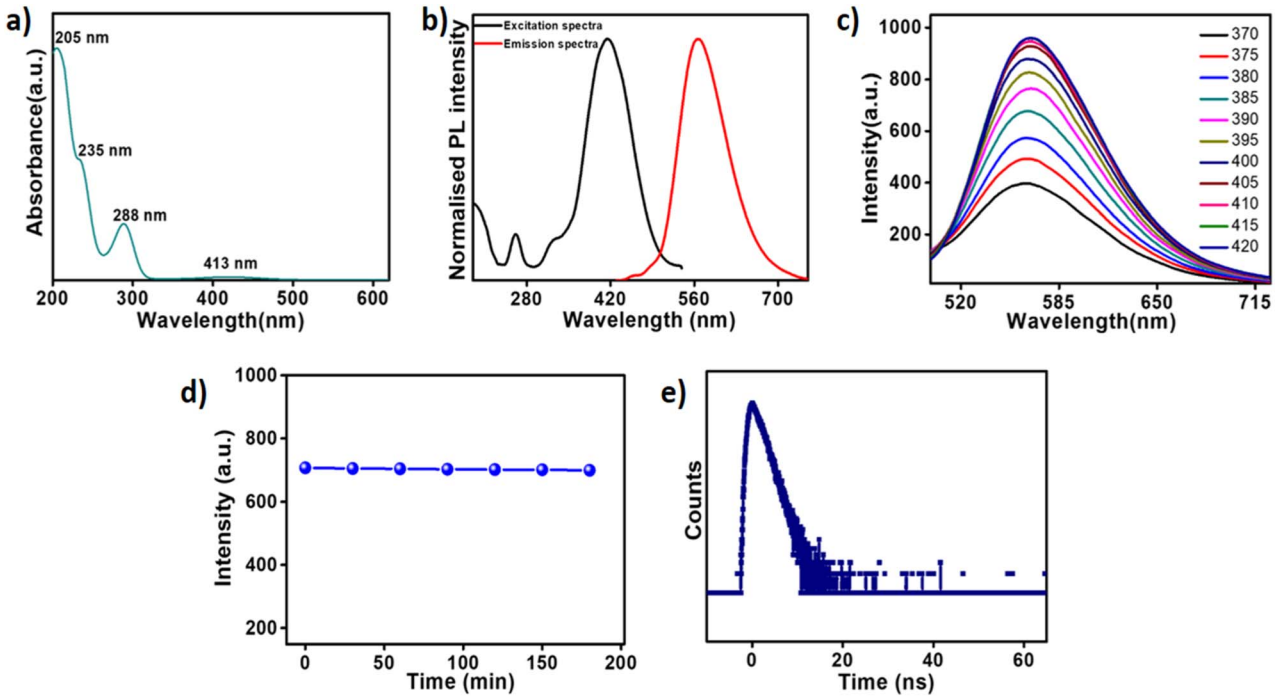

Fig. 2 (a) Characterisation of GOQDs. UV-vis spectrum. (b) Excitation and emission spectrum. (c) Excitation independent emission spectra of GOQDs. (d) Time-dependent luminescence intensity. (e) PL decay curve of GOQDs.

n–π* transitions of C=O bonds.[40,41] The broad absorption around 413 nm is attributed to the n–π* transition of C=O bonds and also indicates the presence of lone pair containing functional groups. These distinct absorption states arise from the variations in the π-conjugated electron system.[42,43] Furthermore, this observation confirms the presence of oxygenated groups within the GOQDs. Fig. 2b shows the excitation and emission spectra, with characteristic wavelengths of 370 and 562 nm, respectively. A detailed photoluminescence (PL) examination using several excitation wavelengths is shown in Fig. 2c. The emission peak at 562 nm remains unchanged when the excitation wavelength is increased from 370 to 420 nm. This excitation-independent PL behavior is associated with smaller surface flaws and more uniform sizes of N-doped GOQDs.[44] These observations align with the TEM results. The system also demonstrated significant photostability (Fig. 2d), with the luminescence intensity exhibiting only a marginal change after 3 hours of continuous UV irradiation. The fluorescence lifetime of GOQDs was measured at room temperature using the TCSPC method, yielding an average lifetime (τ_{av}) of 2.35 ns, as determined from the fluorescence decay curve shown in Fig. 2e.

XPS analysis results (Fig. 3a–d) provide further evidence of the carbon core and functional groups in the particles. The XPS survey spectrum of the GOQDs display three peaks at 300.8, 414.1 and 547.3 eV, corresponding to the C 1s, N 1s and O 1s signals, respectively.

Detailed analysis shows that the synthesized GOQDs consist of C, N and O with relative molar concentrations of 79.24, 12.57 and 8.19%, respectively. The C 1s spectrum (Fig. 3b) features four distinct peaks at 284.1 eV (C=C/–CH), 285.2 eV (C–N bond), 286.1 eV (–C–O bond) and 287.5 eV (–C=O bond). The N 1s spectrum (Fig. 3c) reveals two distinct peaks at 396.6 eV (pyridinic Ns) and 397.9 eV (pyrrolic N).[45] The O 1s spectrum (Fig. 3d) shows three peaks at 529.9 eV, 531.2 eV and 532.5 eV, attributed to C=O, C–OH, C–O–C functional groups, respectively.[46] Thus, the structure of the synthesized GOQDs is confirmed to be a carbon core substituted with pyridinic and pyrrolic nitrogen and anchored with hydroxyl, carboxyl and epoxy groups. The elemental mapping of the composite is provided in Fig. S3, SI.

3.2 GOQDs as SERS substrate

The performance of GOQDs as SERS substrate was examined for the detection of RhB. The SERS enhancement effects of GOQDs substrate is measured with 785 nm laser excitation in the presence of 1 mM RhB, as shown in Fig. 4. Interestingly, a significant enhancement in Raman peaks of RhB at 1648 cm^{-1}, 1508 cm^{-1}, 1364 cm^{-1}, 1194 cm^{-1}, 762 cm^{-1} and 634 cm^{-1} is observed on GOQDs substrate. The enhancement response is probably facilitated by the reduction of non-radiative oxygen-containing functional groups in GOQDs.[20] The SERS enhancement mechanisms are primarily attributed to the electromagnetic enhancement (EM) and chemical enhancement (CM) factors. EM arises from the localized electromagnetic field, mainly in the presence of metallic components, while CM involves charge transfer phenomena. Ling *et al.* reported that π–π stacking between graphene and absorbed molecules can reduce the distance between the molecules and the substrate, promoting efficient charge transfer from the

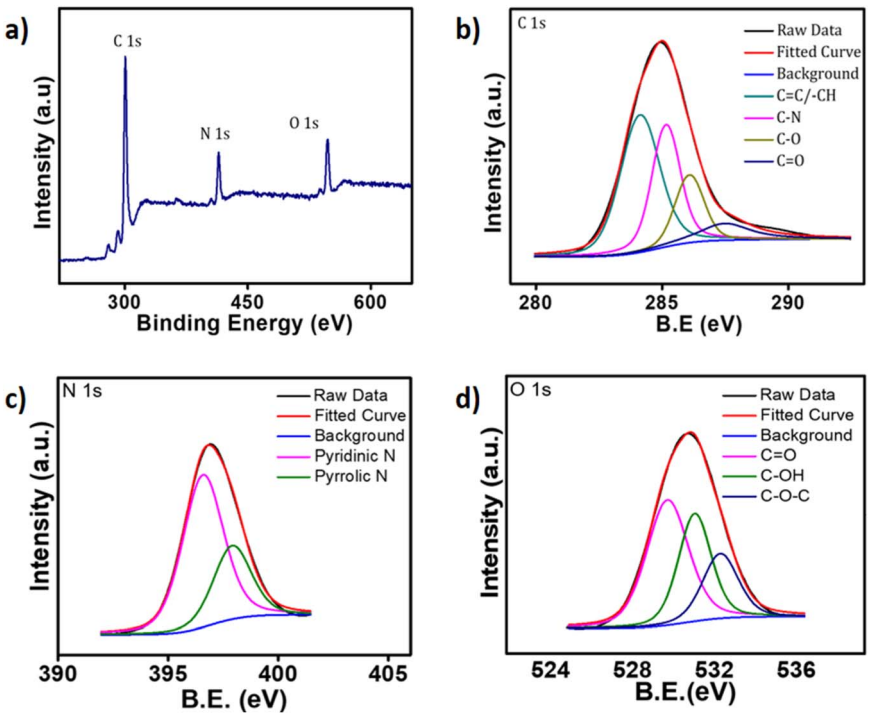

Fig. 3 (a) XPS survey scan of GOQDs. XPS fitting spectra for C 1s (b), N 1s (c), O 1s (d) of GOQDs respectively.

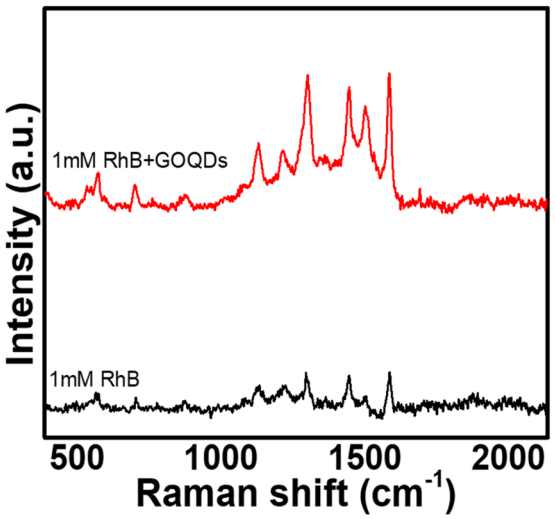

Fig. 4 Raman spectra of 1 mM RhB using GOQDs as SERS substrate.

substrate to the target molecules.[47] In the case of GOQDs, their larger surface areas with more accessible edges and dangling bonds enhance the adsorption of target molecules. Liu *et al.* described the dangling bonds in GOQDs as hot spots that can adsorb or trap RhB molecules.[19] In the current study, the effectiveness of GOQDs as a SERS substrate can be attributed to the following reasons. The sp^2 domains in GOQDs have higher electronic charge content, facilitating maximum charge transfer to the target molecules *via* π–π interaction.[17,20] Due to the high absorption of RhB, strong SERS signal was observed.

3.3 GOQDs as green reducing agent

The inherent reducing capability of GOQDs is often checked for the reduction of metal salts leading to the growth of metallic nanoparticles. The system served as an environmentally benign reducing agent for Pd(II) reduction reaction. The synthesized PdNPs@GOQDs is characterized using XRD analysis, TEM analysis, UV-vis spectroscopy and FT-IR spectroscopy. Digital image showing the brown coloured solution of PdNPs@GOQDs is displayed in Fig. 5a. TEM image of PdNPs@GOQDs given in Fig. 5b–d shows the SAED pattern of the system. The average particles size of PdNPs determined from the HR-TEM analysis was ~2.8 nm. The bare GOQDs were formed as spherical particles with an average size of 2.2 nm as evident from Fig. 1b. In contrast, the PdNPs@GOQDs exhibit a micro sized sheet structure in which the PdNPs with spherical shape were encapsulated by GOQDs (Fig. 5b), revealing that the GOQDs have aggregated and transformed to a sheet during the formation of PdNPs@GOQDs. It is noted that homogeneous dispersion of ultrafine smaller size PdNPs are formed on the surface of GOQDs sheets. Fig. 5c identified the lattice fringes to be 0.22 nm, matching with the previous reports on PdNPs.[26,48,49] The *d*-spacing value calculated from the SAED pattern (Fig. 5d) matches with that of (111) and (311) planes of PdNPs, as derived from the XRD pattern. Fig. 5e shows the XRD pattern of PdNPs@GOQDs, which reveals high crystalline nature of the system. When the peaks characteristic for carbon material are analysed, a striking feature noted was the lower intensity of peaks at 8.5° and 17.5° in comparison with the starting GOQD system, while new peaks are present at 21.9°, 25.7°, 33.4°, 39.7°, 42.5°, 60.2° and 71.6°.[50] Thus it is clear that the addition of Pd(II) changes the structural features of GOQDs. The decrease in the intensity of the first two peaks are likely due to the reduced number of functional groups present. Four Bragg's peaks were obtained at 2θ values 41.2°, 47°, 68.9° and 81.7°, corresponding to (111), (200), (220) and (311) lattice planes of face centered cubic crystal structure for PdNPs. The peak at $2\theta = 41.2°$ is originated due to the f.c.c crystal structure of PdNPs.[48,51,52] XRD analysis and TEM studies thus confirm the formation of PdNPs on GOQDs microsheets. Along with the usual peaks on carbon

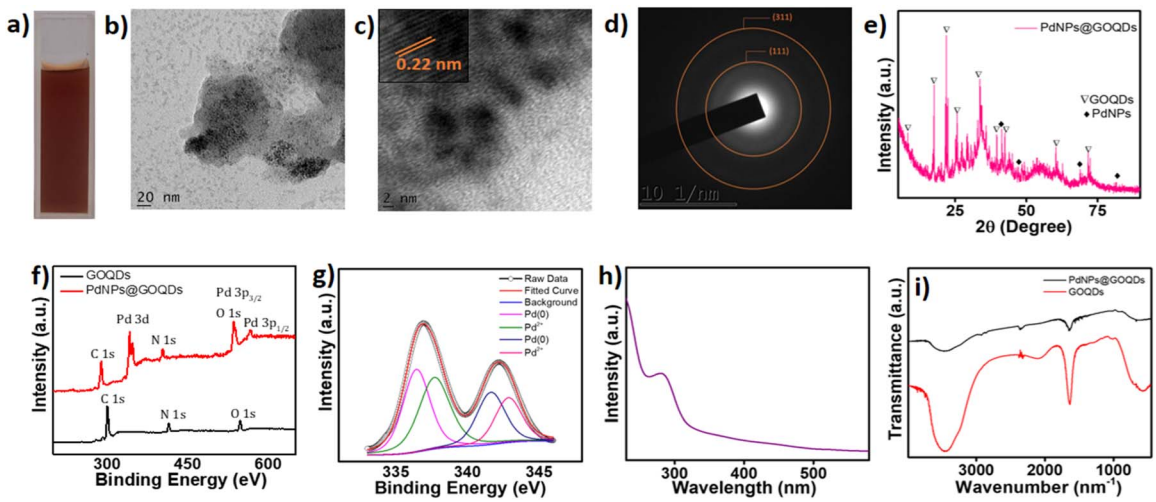

Fig. 5 (a) Photograph of PdNPs@GOQDs. (b) TEM image of PdNPs@GOQDs (c) zoomed TEM image and the lattice fringes. (d) SAED pattern. (e) XRD of PdNPs@GOQDs. (f) Comparison of XPS spectra of GOQDs and PdNPs@GOQDs. (g) Deconvoluted Pd 3d XPS spectra of PdNPs@GOQDs. (h) UV-vis absorption spectrum of PdNPs@GOQDs. (i) Comparison of FT-IR spectra of GOQDs and PdNPs@GOQDs.

core, oxygen and nitrogen, peak originating from Pd (0) is noted at 341.8, 535.7 and 566 eV signifying Pd(3d), Pd($3p_{3/2}$) and Pd($3p_{1/2}$) states in the XPS plot (Fig. 5f and g).[53,54] The peak at 535.7 eV of Pd($3p_{3/2}$) overlaps with binding energy of O 1s. The splitting of Pd(3d) yielded peaks at 336.4 and 341.6 eV corresponding to Pd(0) state (Fig. 5g), assigned respectively to Pd($3d_{5/2}$) and Pd($3d_{3/2}$).[55,56] The additional pair of peaks found at 337.7 and 342.8 eV are indicative of the presence of Pd^{2+} in the solution. UV-vis spectroscopy is extensively used to confirm the synthesis of nanocomposites and nanoparticles, by the corresponding surface plasmon resonance (SPR) peaks. The broadness, intensity and specific position of SPR peak is changed with the change in size and morphology of the nanoparticles. The peak appeared at 280 nm (Fig. 5h) indicates the formation of PdNPs. It is known that the surface plasmon resonance peak of small PdNPs is located in the UV region, resulting in a dark brown color as obtained in the present case (Fig. 5a). These matches with previous results.[52,57,58] A comparison of the FTIR spectra of GOQDs and the PdNPs@GOQDs system is shown in Fig. 5i. Though the spectral patterns are closely similar, the intensities of the bands corresponding to functional groups, particularly oxygen functionalities, have decreased. This decrease in intensity may be attributed to their involvement in the reduction process, vis., to the conversion of Pd(II) to Pd(0).

3.4 Applications of PdNPs@GOQDs

3.4.1 PdNPs@GOQDs as SERS substrate. Metal nanoparticles as well as graphene matrix are well established SERS substrates. To estimate the SERS activity of their combination, vis., the PdNPs@GOQDs, RhB molecule was chosen as the analyte. A significant enhancement in the Raman peaks of RhB at 1648 cm^{-1}, 1508 cm^{-1}, 1364 cm^{-1}, 1194 cm^{-1} and 634 cm^{-1} are observed on PdNPs@GOQDs substrate (Fig. 6a). Compared to GOQDs the signal intensity of the PdNPs@GOQDs substrate is many fold higher, indicating the involvement of PdNPs also in the process. From the perspective of the electromagnetic enhancement mechanism (EM), the enhancement of Raman signal is mainly due to the local electromagnetic fields which is amplified because of the excitation of localized free electrons causing collective oscillation (surface-plasmon resonance) in the metal. The electromagnetic field is highly localized in narrow regions (interparticle or particle–substrate nanogaps), which is called 'SERS hotspots'. These hotspots occupy less than 1% of the total area, but contribute almost 50% of the SERS intensity.[59] From the perspective of chemical enhancement mechanism (CM), the enhancement effect is linked to the degree of contact between the substrate and the target molecules.

GOQDs, with their intrinsic π–π layer structure, allow for closer contact with RhB molecules through π–π stacking. Additionally, while many oxygen functional groups on the surface of the GOQDs are consumed during the formation of PdNPs@GOQDs compounds, some remain on the surface. These groups contribute to the electronegativity and hydrophilicity of GOQDs, improving their ability to adsorb RhB molecules through electrostatic interactions, because RhB is a cationic dye. These two enhancement factors facilitate adsorption of RhB molecules, facilitating charge transfer between PdNPs@GOQDs compounds and RhB molecules, guiding the RhB molecules precisely to the "hot spot" sites, resulting in a higher SERS signal compared to GOQDs alone.[60] Fig. 6b shows the concentration dependent SERS enhancement. The limit of detection of the analyte is found to be 5 μM. The SERS enhancement factor for the composite is found to be 3×10^6. A comparison of the performance with GOQD/metal based systems is given in Table S1, SI. Enhanced performance of PdNPs@GOQDs in SERS activity is evident from a comparison of the system with pure palladium nanoparticles and physically mixed palladium nanoparticles and GOQDs (Fig. S4a, SI). SERS activity of the system is further confirmed using an aromatic nitro compound and pesticide (Fig. S4b and c, SI).

3.4.2 Catalytic activity of PdNPs@GOQDs in reduction reaction. PdNPs@GOQDs system was also examined for their catalytic activity in reduction reactions, for which aromatic nitro compounds were selected as the reactants. To assess this, hydrogenation of 4-nitro phenol (4-NP) was attempted, following the procedure described in Section 2.4. The

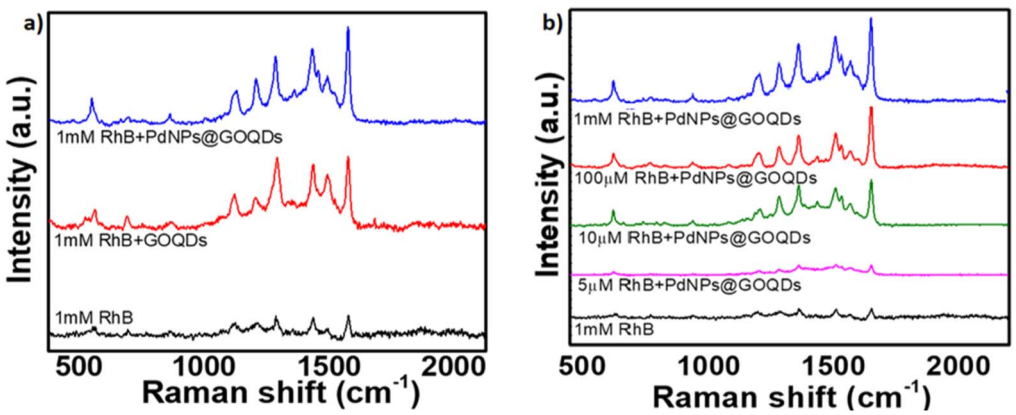

Fig. 6 (a) Comparison of SERS enhancement of analyte signal on GOQDs & PdNPs@GOQDs for RhB. (b) Different concentrations of RhB on PdNPs@GOQDs.

concentration of $NaBH_4$ was maintained 100 fold excess than that of 4-NP during the reaction, so that pseudo-first-order kinetics for the catalysis was ensured. The above-mentioned conversion was indicated by the change in colour of the pale yellow solution to bright yellow. Nitrophenolate ion shows characteristic absorbance at 400 nm, which remained unchanged till the addition of 100 μL PdNPs@GOQDs solution into it. With the introduction of PdNPs@GOQDs, a decrease in the absorbance at the said value was observed, denoting the reduction of 4-NP. Concomitant formation of a new peak around 292 nm was also noticed (Fig. 7), signifying the formation of 4-amino phenol (4-AP), the desired product of hydrogenation of 4-NP, demonstrating the catalytic activity of PdNPs@GOQDs. The possible mechanistic pathway to the product is represented in Fig. S5, SI.

3.4.3 Hydrogenation of nitroarenes using PdNPs@GOQDs. PdNPs@GOQDs are further administered for reducing other significant nitroarenes, to corresponding aminoarenes. Aniline and its derivatives have found widespread applications in the design and synthesis of pharmaceuticals, dyes, polymers, functional materials and supramolecules.[61] As the direct introduction of an amino group onto readily available aromatic feedstock chemicals is impractical, their nitration and subsequent reduction is the most popular approach towards the synthesis of aromatic amines. The reduction of nitroarenes to corresponding anilines are generally carried out *via* homogenous and heterogenous reduction using catalysts based on metals such as Pd, Pt, Rh, Ir, *etc.* Among such methods, Pd-based heterogenous catalysis is especially attractive due to the high levels of selectivity, efficiency and options for catalyst recovery and reuse.

$$\text{R-NO}_2 \xrightarrow[\text{NaBH}_4,\ \text{H}_2\text{O}\ 25\ ^\circ\text{C},\ 30\ \text{min}]{\text{PdNPs@GOQDs}} \text{R-NH}_2$$

The use of Pd-based nano catalysts enhance the above-mentioned advantages due to the favourable virtues of nanoparticles.[67–71] In view of the above, it appeared attractive to test the utility and efficiency of the developed PdNPs@GOQDs nanocatalyst in the reduction reaction of nitroarenes. The experimental aspects concerned are provided in Section 2.5.

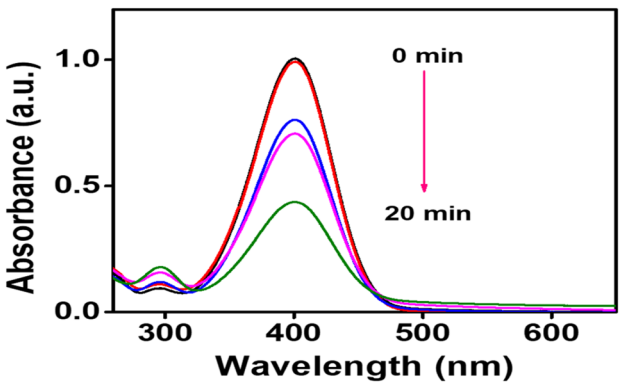

Fig. 7 Change in UV absorbance of 4-NP during the catalytic hydrogenation to 4-AP using PdNPs@GOQDs.

The results of the study are given in Table 1. The NMR data and spectra of the synthesized aniline and its derivatives are provided in Table S2 and Fig. S8, SI. The UV-vis spectral data of the reactants and the products obtained after the reaction are provided in Fig. S6, SI.

As a pilot reaction, the reduction of nitrobenzene to aniline was investigated using the PdNPs@GOQDs as the catalyst, sodium borohydride as hydrogen source in deionised water at room temperature. Pleasingly, in just 30 minutes, nearly quantitative yield of aniline was obtained after work up and isolation of the reaction mixture. Moreover, the PdNPs@GOQDs catalyst was effective in promoting the reduction of a few functionalised nitroarenes as shown in Table 1. Importantly, sensitive functionalities such as nitrile and ester groups were tolerant under the reaction conditions to generate the corresponding anilines in 98% and 70% isolated yields (entries 2 and 5). However, the treatment of 3-nitroacetophenone under identical reaction conditions resulted in global reduction leading to the formation of a secondary alcohol-bearing aniline in 88% yield. At this context, it is reasonable to compare the catalytic activity of PdNPs@GOQDs with other reported

Table 1 Results of Nitro compounds reduction using PdNPs@GOQDs as catalysts

Entry	Substrate	Product	Isolated yield
1	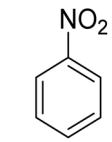	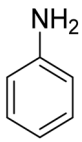	99%
2	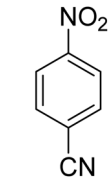	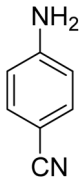	98%
3	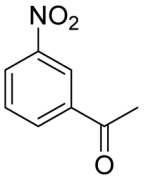	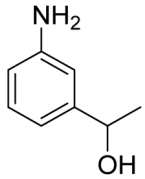	88%
4	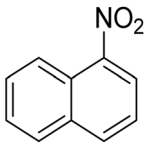	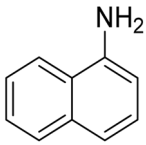	99%
5	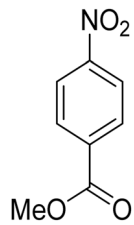	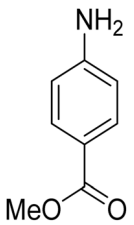	70%

Table 2 Comparison of catalytic activity of various palladium catalysts for the reduction of nitrobenzene

Sl. no.	Catalyst	Solvent	Time (h)	Temperature (°C)	Yield (%)	Ref.
1	Pd-gCN	EtOH	4	70	99	62
2	PdNPs@Cell-N-GQD	H_2O	2	Room temperature	95	29
3	Pd-NPs@Oak Gum	EtOH/H_2O	1	50	96	63
4	PdNPs/RGO	EtOH/H_2O	1.5	50	98	64
5	PdCu/graphene	EtOH/H_2O	1.5	50	95	65
6	Pd/PEG4000	EtOH	1.5	Room temperature	100	66
7	PdNPs@GOQDs	H_2O	0.5	Room temperature	99	Present work

systems. Nitrobenzene reduction is selected as the test reaction. A comparison of reaction conditions, in terms of time, temperature as well as solvent, is presented here (Table 2). It is evident that the present system is definitely a preferable one among the series. The catalyst is reusable up to 5 cycles, as evident from the study conducted using nitrobenzene as reactant (Fig. S7, SI). After five cycles the yield is observed to be 90%.

4 Conclusion

Here, nitrogen doped Graphene Oxide Quantum Dots with yellow luminescence are synthesized from *ortho* phenylenediamine through hydrothermal method. The system is explored as SERS substrate, using Rhodamine B as analyte. The enhancement in the Raman signal is attributed to the significant charge transfer to the target molecules *via* π–π interaction. The reduction capability of GOQDs, made them strong contenders for metal nanoparticle synthesis, as exemplified by the formation of Pd(0) from Pd(II). The presence of oxygen-containing surface functional groups initiates the reduction process, allowing these carbon particles to act as both reducing and stabilizing agents in noble metal nanoparticle synthesis. The SERS effect of PdNPs@GOQDs was analyzed and compared with GOQDs, showing that PdNPs@GOQDs have enhanced SERS effect. The excellent catalytic activity of PdNPs@GOQDs was established using hydrogenation reaction of 4-nitrophenol. Then PdNPs@GOQDs catalyst was further used for the reduction of various functionalized nitroarenes. Sensitive groups such as nitrile and ester were well-tolerant, yielding the corresponding anilines with isolated yields of 98% and 70%, respectively, showing excellent catalytic activity of the system.

Conflicts of interest

There are no conflicts to declare.

Data availability

Data are available upon request from the authors.

Supplementary information (SI): GOQDs formation mechanism, AFM of GOQDs, EDX map of PDNPs@GOQDs, UV-vis spectra of nitroaromatics, the NMR data and spectra of the synthesized aniline and its derivatives. See DOI: https://doi.org/10.1039/d5ra08190d.

Acknowledgements

A. T. P. acknowledges CSIR-UGC for the research fellowship. The authors are grateful to CSIF-University of Calicut, and Department of chemistry-Christ (Deemed to be University) Bengaluru for the analytical support. R. N. K. gratefully acknowledges Government of India, for the research facilities provided under FIST, and the financial assistance obtained under the PAIR programme of ANRF (File No.ANRF/PAIR/2025/000021/PAIR-A).

References

1 Z. Jin, P. Owour, S. Lei and L. Ge, Graphene, graphene quantum dots and their applications in optoelectronics, *Curr. Opin. Colloid Interface Sci.*, 2015, **20**(5–6), 439–453.
2 S. Ahirwar, S. Mallick and D. Bahadur, Electrochemical method to prepare graphene quantum dots and graphene oxide quantum dots, *ACS Omega*, 2017, **2**(11), 8343–8353.
3 V. Ansi, P. Sreelakshmi, R. Poovathinthodiyil and N. Renuka, Table sugar derived carbon dot—A promising green reducing agent, *Mater. Res. Bull.*, 2021, **139**, 111284.
4 P. V. Raveendran and N. Renuka, Carbon dots as a sustainable alternative to plant extracts for the green synthesis of noble metal nanoparticles, *Environ. Nanotechnol. Monit. Manag.*, 2022, **18**, 100676.
5 J. Kneipp, Nanosensors based on SERS for applications in living cells, in. *Surface-enhanced Raman Scattering: Physics and Applications*, Springer, 2006, pp. 335–349.
6 H. K. Lee, Y. H. Lee, C. S. L. Koh, G. C. Phan-Quang, X. Han, C. L. Lay, H. Y. F. Sim, Y.-C. Kao, Q. An and X. Y. Ling, Designing surface-enhanced Raman scattering (SERS) platforms beyond hotspot engineering: emerging opportunities in analyte manipulations and hybrid materials, *Chem. Soc. Rev.*, 2019, **48**(3), 731–756.
7 S. Lee, H. Dang, J.-I. Moon, K. Kim, Y. Joung, S. Park, Q. Yu, J. Chen, M. Lu and L. Chen, SERS-based microdevices for use as *in vitro* diagnostic biosensors, *Chem. Soc. Rev.*, 2024, **53**(11), 5394–5427.
8 B. Ren, G.-K. Liu, X.-B. Lian, Z.-L. Yang and Z.-Q. Tian, Raman spectroscopy on transition metals, *Anal. Bioanal. Chem.*, 2007, **388**, 29–45.
9 M. Fan, G. F. Andrade and A. G. Brolo, A review on the fabrication of substrates for surface enhanced Raman spectroscopy and their applications in analytical chemistry, *Anal. Chim. Acta*, 2011, **693**(1–2), 7–25.

10 L. Bi, X. Wang, X. Cao, L. Liu, C. Bai, Q. Zheng, J. Choo and L. Chen, SERS-active Au@ Ag core-shell nanorod (Au@ AgNR) tags for ultrasensitive bacteria detection and antibiotic-susceptibility testing, *Talanta*, 2020, **220**, 121397.
11 K. Luo, A. Chen, Y. Liu, J. Yang, N. Cai and J. Li, Constructing a highly sensitive SERS sensor based on necklace-like CNC/ZIF-8/Ag to detect and photo-degrade diquat in green tea leaves, *Ind. Crops Prod.*, 2025, **225**, 120453.
12 X. Wen, H. Cheng, W. Zhang, L. You and J. Li, Multifunctional Ni (OH) 2/Ag composites for ultrasensitive SERS detection and efficient photocatalytic degradation of ciprofloxacin and methylene blue, *Talanta*, 2024, **266**, 125140.
13 X. Wen, Y. Liu, W. Zhang, L. You, N. Cai and J. Li, Recyclable NiO/g-C3N4/ag hybrid substrates for sensitive SERS detection and photo-degradation of residual pesticides in beverages, *Food Chem.*, 2025, **464**, 141935.
14 A. K. Geim and K. S. Novoselov, The rise of graphene, *Nat. Mater.*, 2007, **6**(3), 183–191.
15 V. Sharma, N. N. Som, S. B. Pillai and P. K. Jha, Utilization of doped GQDs for ultrasensitive detection of catastrophic melamine: A new SERS platform, *Spectrochim. Acta, Part A*, 2020, **224**, 117352.
16 D. Lin, T. Qin, Y. Wang, X. Sun and L. Chen, Graphene oxide wrapped SERS tags: multifunctional platforms toward optical labeling, photothermal ablation of bacteria, and the monitoring of killing effect, *ACS Appl. Mater. Interfaces*, 2014, **6**(2), 1320–1329.
17 H. Cheng, Y. Zhao, Y. Fan, X. Xie, L. Qu and G. Shi, Graphene-quantum-dot assembled nanotubes: a new platform for efficient Raman enhancement, *ACS Nano*, 2012, **6**(3), 2237–2244.
18 W. Xu, N. Mao and J. Zhang, Graphene: a platform for surface-enhanced Raman spectroscopy, *Small*, 2013, **9**(8), 1206–1224.
19 D. Liu, X. Chen, Y. Hu, T. Sun, Z. Song, Y. Zheng, Y. Cao, Z. Cai, M. Cao and L. Peng, Raman enhancement on ultra-clean graphene quantum dots produced by quasi-equilibrium plasma-enhanced chemical vapor deposition, *Nat. Commun.*, 2018, **9**(1), 193.
20 R. Das, S. Parveen, A. Bora and P. Giri, Origin of high photoluminescence yield and high SERS sensitivity of nitrogen-doped graphene quantum dots, *Carbon*, 2020, **160**, 273–286.
21 M. Keshavarz, A. R. H. Chowdhury, P. Kassanos, B. Tan and K. Venkatakrishnan, Self-assembled N-doped Q-dot carbon nanostructures as a SERS-active biosensor with selective therapeutic functionality, *Sens. Actuators, B*, 2020, **323**, 128703.
22 R. Panyathip, S. Sucharitakul, S. Phaduangdhitidhada, A. Ngamjarurojana, P. Kumnorkaew and S. Choopun, Surface enhanced raman scattering in graphene quantum dots grown *via* electrochemical process, *Molecules*, 2021, **26**(18), 5484.
23 Y. S. Mary and Y. S. Mary, Utilization of doped/undoped graphene quantum dots for ultrasensitive detection of duphaston, a SERS platform, *Spectrochim. Acta, Part A*, 2021, **244**, 118865.
24 S. Ghosh, S. S. Satapathy, K. Ghosh, S. Jauhari, S. K. Panda and S. Si, Carbon Dots Assisted Synthesis of Gold Nanoparticles and Their Catalytic Activity in 4-Nitrophenol Reduction, *ChemistrySelect*, 2019, **4**(12), 3416–3422.
25 X. Wang, R. Zhang, X. Ma, Z. Xu, M. Ma, T. Zhang, Y. Ma and F. Shi, Carbon dots@ noble metal nanoparticle composites: research progress report, *Analyst*, 2024, **149**(3), 665–688.
26 N. Dhenadhayalan, T. H. Hsin and K. C. Lin, Multifunctional Nanohybrid of Palladium Nanoparticles Encapsulated by Carbon-Dots for Exploiting Synergetic Applications, *Adv. Mater. Interfaces*, 2019, **6**(13), 1900361.
27 A. Selim, S. Kaur, A. H. Dar, S. Sartaliya and G. Jayamurugan, Synergistic effects of carbon dots and palladium nanoparticles enhance the sonocatalytic performance for Rhodamine B degradation in the absence of light, *ACS Omega*, 2020, **5**(35), 22603–22613.
28 D. Dey, T. Bhattacharya, B. Majumdar, S. Mandani, B. Sharma and T. K. Sarma, Carbon dot reduced palladium nanoparticles as active catalysts for carbon–carbon bond formation, *Dalton Trans.*, 2013, **42**(38), 13821–13825.
29 S. Keshipour and K. Adak, Pd (0) supported on N-doped graphene quantum dot modified cellulose as an efficient catalyst for the green reduction of nitroaromatics, *RSC Adv.*, 2016, **6**(92), 89407–89412.
30 C. P. Deming, R. Mercado, V. Gadiraju, S. W. Sweeney, M. Khan and S. Chen, Graphene quantum dots-supported palladium nanoparticles for efficient electrocatalytic reduction of oxygen in alkaline media, *ACS Sustain. Chem. Eng.*, 2015, **3**(12), 3315–3323.
31 P. He, J. Bai, F. Qin, X. Wang, X. Yu, Y. Yao and L. Ren, Catalyst regulation of o-phenylenediamine-based carbon dots to achieve single red emission, *Appl. Surf. Sci.*, 2024, **652**, 159367.
32 B. Karimi and B. Ramezanzadeh, A comparative study on the effects of ultrathin luminescent graphene oxide quantum dot (GOQD) and graphene oxide (GO) nanosheets on the interfacial interactions and mechanical properties of an epoxy composite, *J. Colloid Interface Sci.*, 2017, **493**, 62–76.
33 A. Shokry, M. Khalil, H. Ibrahim, M. Soliman and S. Ebrahim, Highly luminescent ternary nanocomposite of polyaniline, silver nanoparticles and graphene oxide quantum dots, *Sci. Rep.*, 2019, **9**(1), 16984.
34 Y. Zhu, Y. Zhu, H. Ni and R. Gu, Preparation and Properties of Nitrogen-doped Graphene Composite Carbon Materials Prepared from Different Nitrogen Sources, *J. Phys.: Conf. Ser.*, 2023, 012089.
35 R. Souza da Costa, W. Ferreira da Cunha, N. Simenremis Pereira and A. Marti Ceschin, An alternative route to obtain carbon quantum dots from photoluminescent materials in peat, *Materials*, 2018, **11**(9), 1492.
36 H. Miao, S. Li, Z. Wang, S. Sun, M. Kuang, Z. Liu and J. Yuan, Enhancing the pyridinic N content of Nitrogen-doped graphene and improving its catalytic activity for oxygen reduction reaction, *Int. J. Hydrogen Energy*, 2017, **42**(47), 28298–28308.

37 P. Wu, W. Li, Q. Wu, Y. Liu and S. Liu, Hydrothermal synthesis of nitrogen-doped carbon quantum dots from microcrystalline cellulose for the detection of Fe 3+ ions in an acidic environment, *RSC Adv.*, 2017, **7**(70), 44144–44153.
38 F. T. Johra, J.-W. Lee and W.-G. Jung, Facile and safe graphene preparation on solution based platform, *J. Ind. Eng. Chem.*, 2014, **20**(5), 2883–2887.
39 A. Y. Lee, K. Yang, N. D. Anh, C. Park, S. M. Lee, T. G. Lee and M. S. Jeong, Raman study of D* band in graphene oxide and its correlation with reduction, *Appl. Surf. Sci.*, 2021, **536**, 147990.
40 Y. Feng, J. Zhao, X. Yan, F. Tang and Q. Xue, Enhancement in the fluorescence of graphene quantum dots by hydrazine hydrate reduction, *Carbon*, 2014, **66**, 334–339.
41 S. Kang, K. M. Kim, K. Jung, Y. Son, S. Mhin, J. H. Ryu, K. B. Shim, B. Lee, H. Han and T. Song, Graphene oxide quantum dots derived from coal for bioimaging: facile and green approach, *Sci. Rep.*, 2019, **9**(1), 4101.
42 Z.-H. Wen and X.-B. Yin, Excitation-independent carbon dots, from photoluminescence mechanism to single-color application, *RSC Adv.*, 2016, **6**(33), 27829–27835.
43 P. Varatharajan, I. S. Banu, M. H. Mamat and N. Vasimalai, Hydrothermal synthesis of orange fluorescent carbon dots and their application in fabrication of warm WLEDs and fluorescent ink, *Phys. B*, 2023, **654**, 414703.
44 M. Vedamalai, A. P. Periasamy, C.-W. Wang, Y.-T. Tseng, L.-C. Ho, C.-C. Shih and H.-T. Chang, Carbon nanodots prepared from o-phenylenediamine for sensing of Cu 2+ ions in cells, *Nanoscale*, 2014, **6**(21), 13119–13125.
45 B. Vinayan, N. I. Schwarzburger and M. Fichtner, Synthesis of a nitrogen rich (2D–1D) hybrid carbon nanomaterial using a MnO 2 nanorod template for high performance Li-ion battery applications, *J. Mater. Chem. A*, 2015, **3**(13), 6810–6818.
46 L. Sun, Z. Mo, Q. Li, D. Zheng, X. Qiu and X. Pan, Facile synthesis and performance of pH/temperature dual-response hydrogel containing lignin-based carbon dots, *Int. J. Biol. Macromol.*, 2021, **175**, 516–525.
47 X. Ling, L. Xie, Y. Fang, H. Xu, H. Zhang, J. Kong, M. S. Dresselhaus, J. Zhang and Z. Liu, Can graphene be used as a substrate for Raman enhancement?, *Nano Lett.*, 2010, **10**(2), 553–561.
48 M. Khan, M. R. Shaik, S. F. Adil, M. Kuniyil, M. Ashraf, H. Frerichs, M. A. Sarif, M. R. H. Siddiqui, A. Al-Warthan and J. P. Labis, Facile synthesis of Pd@ graphene nanocomposites with enhanced catalytic activity towards Suzuki coupling reaction, *Sci. Rep.*, 2020, **10**(1), 11728.
49 E. Coronado, A. Ribera, J. García-Martínez, N. Linares and L. M. Liz-Marzán, Synthesis, characterization and magnetism of monodispersed water soluble palladium nanoparticles, *J. Mater. Chem.*, 2008, **18**(46), 5682–5688.
50 M. Goswami, S. Mandal and V. K. Pillai, Effect of hetero-atom doping on the electrocatalytic properties of graphene quantum dots for oxygen reduction reaction, *Sci. Rep.*, 2023, **13**(1), 5182.
51 K. Mohammadnezhad, F. Ahour and S. Keshipour, Electrochemical determination of ascorbic acid using palladium supported on N-doped graphene quantum dot modified electrode, *Sci. Rep.*, 2024, **14**(1), 5982.
52 S. Ullah, A. Ahmad, A. Khan, J. Zhang, M. Raza, A. ur Rahman, M. Tariq, S. Zada and Q. Yuan, Palladium nanoparticles synthesis, characterization using glucosamine as the reductant and stabilizing agent to explore their antibacterial & catalytic applications, *Microb. Pathog.*, 2018, **125**, 150–157.
53 J. Chastain and R. C. King Jr, *Handbook of X-Ray Photoelectron Spectroscopy*, Perkin-Elmer Corporation, 1992, vol. 40, p. 221.
54 S. Yang, J. Dong, Z. Yao, C. Shen, X. Shi, Y. Tian, S. Lin and X. Zhang, One-pot synthesis of graphene-supported monodisperse Pd nanoparticles as catalyst for formic acid electro-oxidation, *Sci. Rep.*, 2014, **4**(1), 4501.
55 C. Lu, Q. Zhu, X. Zhang, H. Ji, Y. Zhou, H. Wang, Q. Liu, J. Nie, W. Han and X. Li, Decoration of Pd nanoparticles with N and S doped carbon quantum dots as a robust catalyst for the chemoselective hydrogenation reaction, *ACS Sustain. Chem. Eng.*, 2019, **7**(9), 8542–8553.
56 C. Lu, M. Wang, Z. Feng, Y. Qi, F. Feng, L. Ma, Q. Zhang and X. Li, A phosphorus–carbon framework over activated carbon supported palladium nanoparticles for the chemoselective hydrogenation of para-chloronitrobenzene, *Catal. Sci. Technol.*, 2017, **7**(7), 1581–1589.
57 C. Chen, J. Wang and Y. Gao, Wavelength-Dependent Nonlinear Absorption in Palladium Nanoparticles, *Appl. Sci.*, 2021, **11**(4), 1640.
58 A. Omidvar, M. RashidianVaziri, B. Jaleh, N. P. Shabestari and M. Noroozi, Metal-enhanced fluorescence of graphene oxide by palladium nanoparticles in the blue–green part of the spectrum, *Chin. Phys. B*, 2016, **25**(11), 118102.
59 M. Rakibuddin and H. Kim, Facile green syntheses of palladium nanoparticles using fruit and aloe vera juices, and their surface–enhanced Raman scattering (SERS) activities, *Mater. Res. Express*, 2018, **5**(8), 085001.
60 J. Ge, Y. Li, J. Wang, Y. Pu, W. Xue and X. Liu, Green synthesis of graphene quantum dots and silver nanoparticles compounds with excellent surface enhanced Raman scattering performance, *J. Alloys Compd.*, 2016, **663**, 166–171.
61 Z. Rappoport, *The Chemistry of Anilines, Part 1*, John Wiley & Sons, 2007.
62 D. Nandi, S. Siwal, M. Choudhary and K. Mallick, Carbon nitride supported palladium nanoparticles: An active system for the reduction of aromatic nitro-compounds, *Appl. Catal., A*, 2016, **523**, 31–38.
63 H. Veisi, N. H. Nasrabadi and P. Mohammadi, Biosynthesis of palladium nanoparticles as a heterogeneous and reusable nanocatalyst for reduction of nitroarenes and Suzuki coupling reactions, *Appl. Organomet. Chem.*, 2016, **30**(11), 890–896.
64 M. Nasrollahzadeh, S. M. Sajadi, A. Rostami-Vartooni, M. Alizadeh and M. Bagherzadeh, Green synthesis of the Pd nanoparticles supported on reduced graphene oxide using barberry fruit extract and its application as

a recyclable and heterogeneous catalyst for the reduction of nitroarenes, *J. Colloid Interface Sci.*, 2016, **466**, 360–368.

65 Y.-S. Feng, J.-J. Ma, Y.-M. Kang and H.-J. Xu, PdCu nanoparticles supported on graphene: an efficient and recyclable catalyst for reduction of nitroarenes, *Tetrahedron*, 2014, **70**(36), 6100–6105.

66 F. Harraz, S. El-Hout, H. Killa and I. Ibrahim, Palladium nanoparticles stabilized by polyethylene glycol: Efficient, recyclable catalyst for hydrogenation of styrene and nitrobenzene, *J. Catal.*, 2012, **286**, 184–192.

67 B. Lakshminarayana, M. Selvaraj, G. Satyanarayana and C. Subrahmanyam, Switching of support materials for the hydrogenation of nitroarenes: A review, *Catal. Rev.*, 2024, **66**(1), 259–342.

68 P. M. Uberman, C. S. García, J. R. Rodríguez and S. E. Martín, PVP-Pd nanoparticles as efficient catalyst for nitroarene reduction under mild conditions in aqueous media, *Green Chem.*, 2017, **19**(3), 739–748.

69 Z. Yan, X. Xie, Q. Song, F. Ma, X. Sui, Z. Huo and M. Ma, Tandem selective reduction of nitroarenes catalyzed by palladium nanoclusters, *Green Chem.*, 2020, **22**(4), 1301–1307.

70 E. Arenas-Sánchez, C. E. Niño González, V. Resendiz-Bujaidar, E. Smolentseva and B. Acosta, Reduction of Nitroarenes Using Efficient PdRu@ mSiO2 Nanocatalyst Synthesized by a One-Pot Approach, *Adv. Mater. Interfaces*, 2024, **11**(18), 2400055.

71 K. Hasan, I. A. Shehadi, R. G. Joseph, S. P. Patole and A. Elgamouz, β-Cyclodextrin-Functionalized Fe3O4-Supported Pd-Nanocatalyst for the Reduction of Nitroarenes in Water at Mild Conditions, *ACS Omega*, 2023, **8**(26), 23901–23912.